Snakuscules

Philippe Thévenaz and Michael Unser, *Fellow, IEEE*

***Abstract*—A snakuscule (a minuscule snake) is the simplest active contour that we were able to design while keeping the quintessence of traditional snakes: an energy term governed by the data, and a regularization term. Our construction is an area-based snake, as opposed to curve-based snakes. It is parameterized by just two points, thus further easing requirements on the optimizer. Despite their ultimate simplicity, snakuscules retain enough versatility to be employed for solving various problems such as cell counting and segmentation of approximately circular features. In this paper, we detail the design process of a snakuscule and illustrate its usefulness through practical examples. We claim that our didactic intentions are well served by the simplicity of snakuscules.**

***Index Terms*—Curve fitting, geometric modeling, image region analysis, image shape analysis, object detection, parameter estimation, position measurement, size measurement.**

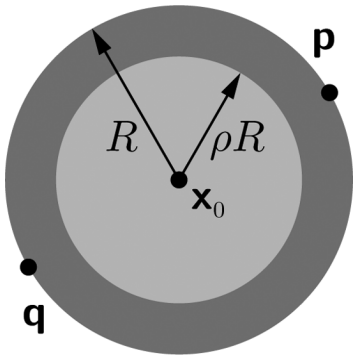

Fig. 1. Snakuscule defined by the two points $\mathbf{p}$ and $\mathbf{q}$. Here, the mouth is light gray and the coils are dark gray.

I. Introduction

Sed qui bellus homo est, Cotta, pusillus homo est [1].[1]

This is the saying that we had in mind while preparing a lecture on snakes—of the image-processing variety. To fulfill our pedagogical ambition, we wanted to illustrate several energy terms, like contour energies or region energies, that would be as simple as possible while remaining nontrivial. We found out that two points were sufficient to define a minuscule snake that would satisfy our needs: the snakuscule—a vernacular name for members of the *Serpentuloidæ* superfamily. Despite this low complexity, we were able to associate with it both image-dependent terms and regularization. Moreover, our snakuscule is amenable to the computation of explicit gradients, of which competent optimizers can take advantage.

While our primary goal was didactic, it was a delightful surprise to discover that our new-born snakuscule is a lively animal that can efficiently solve common tasks such as preying on bright blobs, its favorite staple. This is due to its body plan shown in Fig. 1: an inner disk (the mouth) surrounded by an outer adjoining annulus (the coils). Being *Constrictor*-like, the snakuscule excels at ensnaring highly nutritious food (high-intensity pixels) surrounded by less savory nutriments (low-intensity pixels). It continuously adapts its two parameters $\mathbf{p}$ and $\mathbf{q}$ until its mouth gets the most tasty part of a morsel while its coils do the work and get nothing.

Manuscript received November 7, 2006; revised October 30, 2007. The associate editor coordinating the review of this manuscript and approving it for publication was Dr. Mario A. T. (G. E.) Figueiredo.

The authors are with the École polytechnique fédérale de Lausanne (EPFL), Biomedical Imaging Group, CH-1015 Lausanne VD, Switzerland (e-mail: philippe.thevenaz@epfl.ch).

Color versions of one or more of the figures in this paper are available online at http://ieeexplore.ieee.org.

Digital Object Identifier 10.1109/TIP.2007.914742

[1]Small is beautiful.

Translated in technical terms, the snakuscule minimizes a region-based energy that balances the weighted inner area against the weighted outer area. The weights are directly set to the image values, with a positive sign for the annulus and a negative sign for the disk. The energy to minimize is

$$E_{\text{archaeus}} = \int\int_{\rho R<\|\mathbf{x}-\mathbf{x}_0\|<R} f(\mathbf{x})dx_1dx_2 - \int\int_{\|\mathbf{x}-\mathbf{x}_0\|<\rho R} f(\mathbf{x})dx_1dx_2 \quad (1)$$

where f is an image, where $R = (1/2)\|\mathbf{p}-\mathbf{q}\|$ is the outer radius of the snakuscule, where $\mathbf{x}_0 = (\mathbf{p}+\mathbf{q})/2$ gives the location of its spinal chord, and where $0 < \rho < 1$ determines the disk-to-annulus ratio.

II. Darwinian Evolution

There are many families of real snakes with widely varying preying and locomotion habits. The *Leptotyphlopidæ* are small burrowers that live underground. The *Colubridæ Chrysopelea* are able to glide with a surprisingly good aerodynamic efficiency [2]. The *Hydrophidæ* live at sea.

For its part, the snakuscule lives on a 2-D plain and is generally considered a cute animal, unlike real snakes that sometimes elicit the YR (yelling reaction [3]) in ophiophobes. Snakuscule subgenera are recognized by their ρ factor; most subgenera are today extinct (e.g., *Serpentulus archaeus*) in reason of the selective pressure exerted by flat image areas. Here is why: in order for a snakuscule to survive a journey through a region characterized by a constant value, which is known to exist in common images, the animal should neither blow up [4] nor collapse to a singularity [5]. Because the snakuscule minimizes (1), it is vital that the two energy subterms cancel each other when $\forall\, \mathbf{x} \in \mathbb{R}^2 : f(\mathbf{x}) = f_0$. Therefore, only those snakuscules that happened to possess a mouth with an area equal to that of their coils could evolve to this day, like *Serpentulus campester* did. It can be checked that the fittest snakuscule has $\rho = \sqrt{1/2}$, a ratio

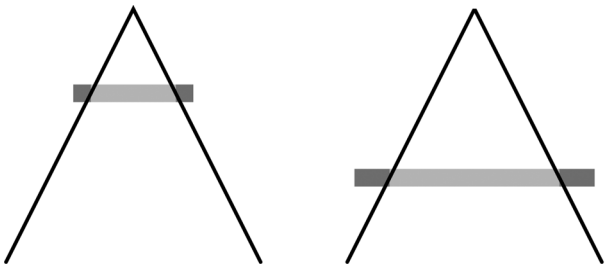

Fig. 2. Feeding snakuscule in cross section, with the horizontal axis representing a space dimension and the vertical axis representing the intensity dimension. The configuration on the right can be interpreted either as a zoom of the left configuration, or as a snakuscule sitting lower on the cone.

that is enjoyed by the *campester* specimen shown in Fig. 1. Its purpose in life is to minimize

$$E_{\text{campester}} = \int\int_{\|\mathbf{x}\|<R} f(\mathbf{x}+\mathbf{x}_0)dx_1dx_2 - 2\int\int_{\|\mathbf{x}\|<R/\sqrt{2}} f(\mathbf{x}+\mathbf{x}_0)dx_1dx_2.$$

III. Scale Invariance

Snakuscules in flat or tilted deserts like to laze in the sun rather than to actively forage, even in the presence of undulating dunes, as evidenced in Appendix A. There, it is seen that a snakuscule will stop crawling if the gradient of its surrounding landscape takes the form (9). However, even if it has stopped crawling, the snakuscule is still free to expand or shrink.

Predators of the snakuscule exploit this weakness and bait traps with conical blobs or lay down conical pits on the 2-D plain. In its blob-hunting frenzy, an unwary snakuscule may pounce on a pyramidal cone and start devouring this toxic prey. What happens then depends on its subgenus. If, like *Serpentulus campester*, it minimizes the energy exactly as expressed in (1) with $\rho = \sqrt{1/2}$, then the snakuscule is doomed by its greed: it will expand forever since the imbalance between the two energy subterms in (1) grows unchecked. For the opposite reason, it would also meet its end at the bottom of a conical pit [6].

Unsophisticated snakuscules perceive the right part of Fig. 2 as more favorable than the left one, while more evolved snakuscules, like *Serpentulus robustus*, avoid being tricked by a cone or a pit and normalize their energy. They perceive the two sides of Fig. 2 as the same situation, up to a zoom factor. They replace (1) by

$$E_{\text{robustus}} = \frac{E_{\text{campester}}}{4R^2} \tag{2}$$

and, thus, favor neither side of Fig. 2. As the snakuscule scholar might be intrigued by the preference of *Serpentulus robustus* for a normalization in R^2, we provide a technical explanation in Appendix B.

IV. Taming a Snakuscule

Snakuscules in the wild exhibit a certain disregard for social conventions. They might optimize (1) or (2) without manners, taking oblique bites, like shown in Fig. 1. This feral attitude is not found in *Serpentulus domesticus*, which can be trained to sit upright to maintain level $\mathbf{p} = (p_1, p_2)$ and $\mathbf{q} = (q_1, q_2)$, so that $p_2 = q_2$. The educated snakuscule unambiguously defines an optimal feeding posture by minimizing

$$E_{\text{domesticus}} = E_{\text{robustus}} + \lambda\frac{(p_2-q_2)^2}{4R^2}. \tag{3}$$

The positive number λ acts as a regularization parameter that distinguishes between the several snakuscule subspecies that are endemic to certain types of images. Typically, high-contrast images are populated with high-λ subspecies.

V. The Common Snakuscule

Snakuscule spotters know all too well that their center of interest is an elusive animal, despite the fact that it is short-sighted and perceives only a very local view of its environment, like the blind *Leptotyphlopidæ* of Section II. Snakuscules initiate crawling movements of $\mathbf{p}$ or $\mathbf{q}$ on the basis of $\nabla E_{\text{domesticus}}$, a component of which is given in Appendix C. While the stimulus (10) can be computed explicitly for a suitable f, the snakuscules described up to now struggle to do this and have rarefied. Due to the Leibniz integral rule, they depend in part on an infinitesimally narrow band; this extreme shortsightedness is also a threat to their survival.

Fortunately, random mutations have resulted in the replacement of the snaking sign $\int$ by the adder sign $\sum$. The subgenus of those mutated snakuscules is *Serpentulus vulgaris*; they minimize

$$E_{\text{vulgaris}} = \frac{1}{\|\mathbf{p}-\mathbf{q}\|^2}\sum_{\mathbf{k}\in\mathbb{Z}^2, r<R+\Delta R/2} s(r)f(\mathbf{k}) + \lambda\frac{(p_2-q_2)^2}{4R^2} \tag{4}$$

where $r = \|\mathbf{k}-\mathbf{x}_0\|$. The function s describes the digestive tract of the snakuscule and tells apart several species, such as *S. vulgaris angulatus* and *S. vulgaris sinuosus*. These species find their way according to the incentive of

$$\frac{\partial E_{\text{vulgaris}}}{\partial p_1} = \frac{-2(p_1-q_1)}{\|\mathbf{p}-\mathbf{q}\|^4}\sum_{\mathbf{k}\in\mathbb{Z}^2, r<R+\Delta R/2} s(r)f(\mathbf{k}) + \frac{1}{\|\mathbf{p}-\mathbf{q}\|^2}\sum_{\mathbf{k}\in\mathbb{Z}^2, r<R+\Delta R/2}\frac{\partial s(r)}{\partial p_1}f(\mathbf{k}) - \lambda\frac{(p_1-q_1)(p_2-q_2)^2}{8R^4} \tag{5}$$

which is more accessible than (10). In particular, members of the *Serpentulus vulgaris* genus are frugal and spare themselves the need for the knowledge of ∇f.

VI. Physiology of a Snakuscule

We show in Fig. 3 a characteristic $s_{\text{angulatus}}(r)$. From left to right, we recognize the spinal chord, the mouth area, the throat, the coils area, and the fangs. Whenever the overall footprint $(2R)$ of a snakuscule grows larger or smaller, the width $\left(\sqrt{2}R\right)$ of its gape follows suite. Meanwhile, the opening Δr of the throat and the length ΔR of the fangs do not; they are set at birth. Typically, the throat extends over $\Delta r = \Delta R/\sqrt{2}$. Thus equipped, snakuscules are resilient to journeys over flat

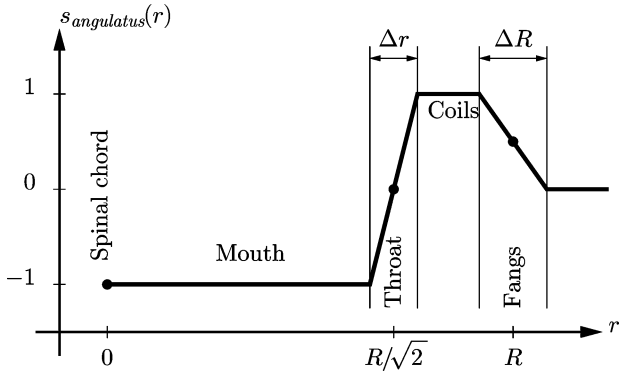

Fig. 3. Digestive tract of *S. vulgaris angulatus*.

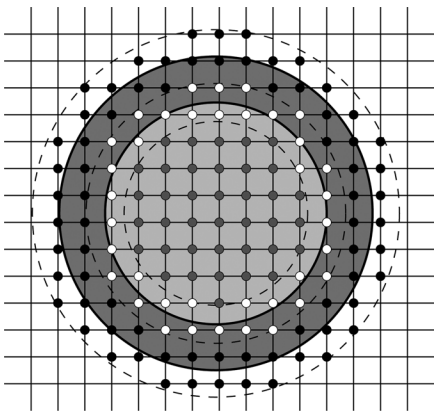

Fig. 4. Arbitrarily located snakuscule with $\Delta r = \sqrt{2}$, $\Delta R = 2$, and $R = 3 + 2\sqrt{2}$. This agonizing snakuscule cannot shrink any smaller lest its coils vanish. Samples taken over the mouth, the throat, and the fangs, are shown in gray, white, and black, respectively.

areas since it can be verified that, with these values, these hardy animals satisfy $\int_0^\infty s_{\text{angulatus}}(r) r dr = 0$. As a side effect, this enforces $R > \Delta r \left(2 + 3\sqrt{2}/2\right)$, a size below which the snakuscule loses coils and life. In Fig. 4, we witness a collapsing *Serpentulus vulgaris* that remains barely alive; should it shrink any further, the fangs would rip its own throat apart—a gruesome demise for a snakuscule.

Our limbless snakuscules use their fangs also as tactile organs. Through them, they apprehend their immediate environment and are drawn to the most nutritive image areas, since $\dot{s}(r) \neq 0$ near $r = R$. Once the coils are wound, the fangs snap and prey is engulfed in the throat—the second organ where $\dot{s}$ contributes. The remaining sections of the snakuscule (the mouth and the coils) exhibit a neutral $\dot{s}_{\text{angulatus}}$, which reduces computational demands.

In contrast to *S. vulgaris angulatus*, the particularity of the *S. vulgaris sinuosus* species is that its digestive tract s_{sinuosus} is continuously differentiable. The evolutionary advantage is a better perception of the environment, but it comes at the cost of higher metabolic needs since more numerous terms contribute to (5) than for *S. vulgaris angulatus*. A breed where this trait is particularly developed is the dog (difference of Gaussians), for example one that satisfies $s_{\text{dog}}(r) = 4^{-r^2/R^2} - 2(16^{-r^2/R^2})$, the only dog specimen that exhibits the desirable traits $s_{\text{dog}}(0) = -1$, $s_{\text{dog}}(R/\sqrt{2}) = 0$, and $\int_0^\infty s_{\text{dog}}(r) r dr = 0$. This last property states that dogs have an all-encompassing wisdom that extends all the way to infinity, but dogs' god-like abilities come at the price of an infinite contemplative time before any move is undertaken. Common snakuscules are much more lively.

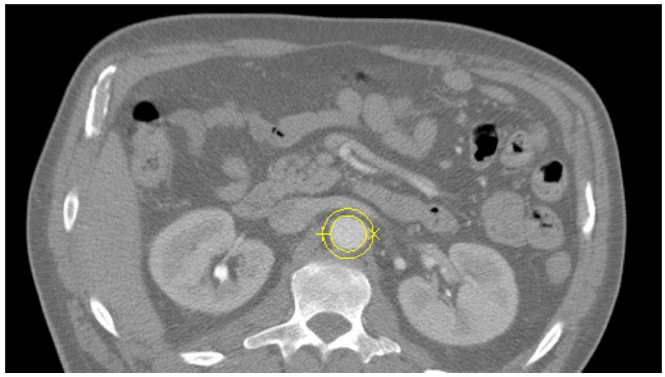

Fig. 5. Snakuscule munching the aorta in a CT slice of a human upper body. A radio-opaque contrast agent has been used as a fertilizer to promote brightness of this artery. Tilling has been achieved by median filtering followed by mild Gaussian smoothing. The small crosses indicate the location of $\mathbf{p}$ and $\mathbf{q}$.

VII. Livestock Snakuscules

A. Stalkers

Snakuscules can benefit their owners in several ways. We present here a case study where they graze on a series of transverse CT slices of a human upper body, where a radio-opaque contrast agent has previously been injected to brighten the main arteries. A pair of snakuscules were shepherded to the approximate location of the left and right iliac artery in one of the low slices. They were then allowed to pursue this quarry; once ensnared, their location and size was recorded and they were translocated to a higher slice. This process went on until the two snakuscules met at the aorta.

Many animal species can coordinate their activity using long-range sensors such as sight [7]; snakuscules cannot. Therefore, their social life is much reduced. Although two snakuscules might tolerate some benign amount of overlap, their direct encounter is, however, lethal. Taking turns, they ram each other until one of them—the winner—can claim a better success, as measured by a minimal E_{vulgaris}. The loser instantly decomposes and vanishes. Consequently, only one snakuscule survived the encounter at the aorta, which it then chased through the remaining upper slices. We show in Fig. 5 the survivor as a set of two yellow circles that summarize fangs and throat.

The recorded trajectory and slice-dependent radii of the snakuscules define the tube shown in Fig. 6. As the CT slices are nearly perpendicular to the aorta, the fact that snakuscules live on a 2-D plain and do not perceive the full 3-D world is mostly harmless.

Region growing of some sort is often at the core of most of the algorithms that undertake the segmentation of the aorta. To be successful, this segmentation should ignore the efferent arteries, which is difficult to achieve with region growing. Moreover, spurious leaks may result from partial-volume effects and

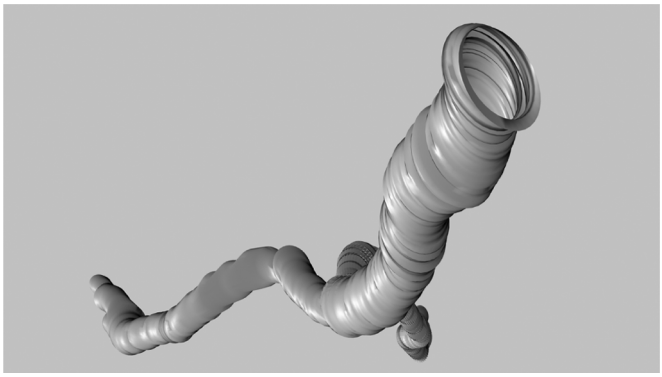

Fig. 6. Snakuscule trails delineating the aorta and two iliac arteries.

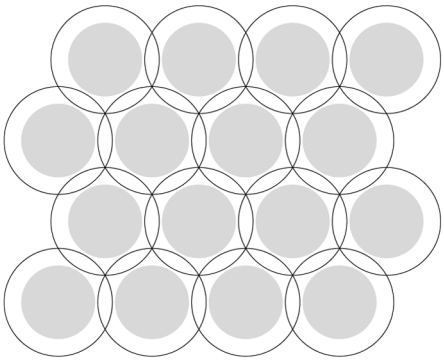

Fig. 7. Swarm of snakuscules in *apis* configuration. The distance between any two neighboring snakuscules is $\sqrt{3}R$. In this configuration, the coils reach everywhere, but not the mouths.

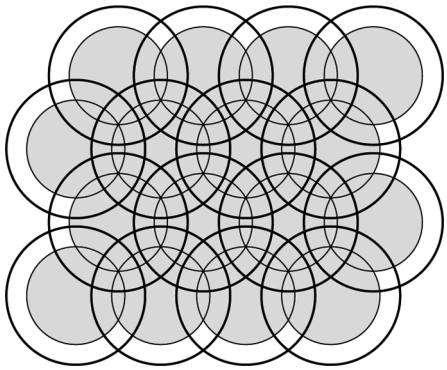

Fig. 8. Swarm of snakuscules in *lupus* configuration. The distance between any two neighboring snakuscules is $\sqrt{(3/2)}R$. In this configuration, no hideout can escape the hungry mouths of the snakuscules.

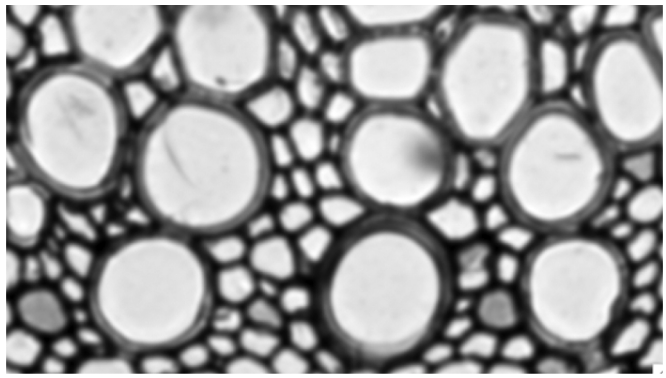

Fig. 9. Slice of dicotyledon, with $10\times$ magnification.

need to be plugged. The use of snakuscules efficiently solves both problems at the same time.

B. Swarm of Snakuscules

A lonesome snakuscule can only do so much; thus, to ransack the plain with more efficiency, snakuscules are known to sometimes congregate. The resulting pack methodically scours the feeding grounds and leaves no hideout. Once deployed, each unit occupies the cell of a hexagonal grid and besieges bright blobs everywhere. The original cell size is chosen according to previously gathered intelligence about the expected dimension of the preys. We show in Fig. 7 a swarm of snakuscules hovering in loose formation. Should this formation break up any further, some territory might escape the attention of the pack. An even tighter formation can be seen in Fig. 8, where no turf is left unchallenged.

At a hissing signal, all snakuscules simultaneously assault their assigned position. When two or more happen to latch onto the same prey, fierce competition ensues, triggered by an intimacy $\|\mathbf{x}_0'' - \mathbf{x}_0'\|$ falling below the escape distance $(1/\sqrt{2})\max(R'', R')$. Only the best snakuscule survives such encounters, as measured by the minimal energy $\min(E''_{\text{vulgaris}}, E'_{\text{vulgaris}})$ attained so far; such jousts are detailed in Appendix D. Once the immediate challengers have vanished, the surviving snakuscule resumes optimizing E_{vulgaris}. In the end, as the amount of loot varies from place to place, some ravenous snakuscules end up with a remaining hunger that exceeds a satiation threshold; those ultimately starve to death.

To illustrate this process, we show in Fig. 9 a luscious place characterized by its riches of bright blobs. It is a microscopy image of a dicotyledon plant magnified ten times, with a variety of cell shapes and sizes, to which a compact swarm of snakuscules is seen flocking in Fig. 10. We show in Fig. 11 the final configuration where the conflicts between snakuscules have been resolved, where all of them have found their optimal feeding posture, and where starvation has taken its toll. We observe that few are the bright blobs that escaped the voracity of the snakuscules. The departure from circularity needs to be pronounced to be an efficient countermeasure. The size mismatch between initial deployment and final configuration seems also to be a poor deterrent, although it occasionally takes a pack of snakuscules to devour large preys (e.g., see top-right corner of Fig. 11). Finally, we conclude that the methodic plundering exerted by a swarm of snakuscules is very efficient at uncovering the location and extent of circular bright blobs for a considerable range of sizes.

VIII. Field Trip

In this section, we examine how our snakuscule construct relates to other deformable templates. It is dedicated to highbrow scientists.

A. Circle Detection by Top-Hat Filter

The energy term (1) of our proposed snakuscule is very similar to the response of a top-hat morphological filter. Such filters have already been used with success to detect circular spots

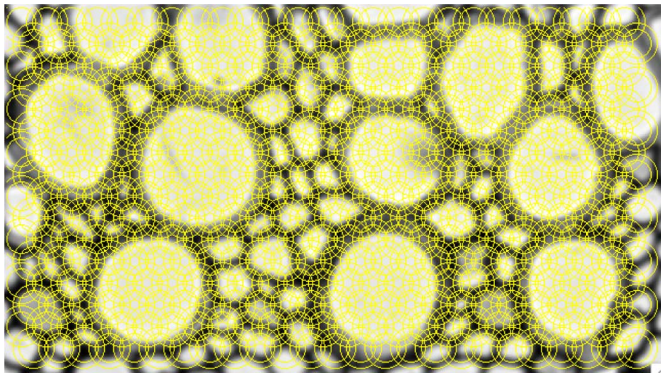

Fig. 10. Initial configuration of a swarm of snakuscules. Here, there are 400 of them, each one 40 pixels wide. They cover most of an image of size (640×360).

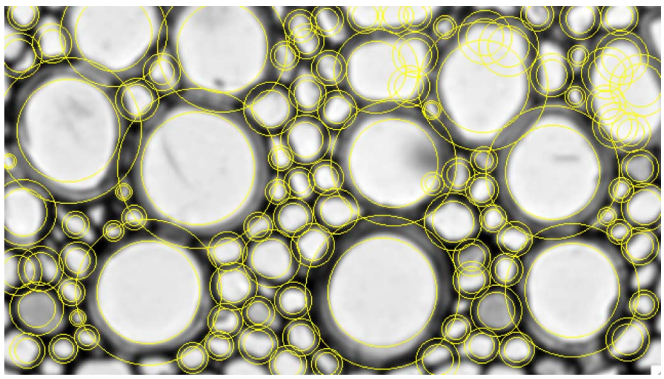

Fig. 11. Final configuration of the swarm of snakuscules. There were 104 survivors.

from images [8]. One novelty of our snakuscule is that we have proposed in (4) a way to allow for continuously varying both the position and the size of the filter; moreover, we have proposed in (5) a formulation where we analytically determine the gradient of the response of the filter with respect to its defining parameters. Neither is possible within the traditional framework of mathematical morphology.

B. Circle Detection by Hough Transform

The Hough transform is a method that was originally designed to characterize straight lines from binary images [9]. A parametric space is first established where any given combination of parameters describes a specific straight line (e.g., slope and intercept). This space is quantized; moreover, each discrete position in this parametric space is provided with a counter initially set to zero. The parametric space is then populated in the following fashion: The collection of all possible virtual lines passing through a single given foreground point within the binary image is considered, and one vote is given to each of their descriptions in the space of parameters; then, the process resumes with the next foreground point. The parameter that receives the majority of votes describes the line that goes through the largest collection of foreground points of the binary image.

It was suggested in [10] that this method could be extended to detect circles; an early implementation can be found in [11]. The method was later generalized to detect arbitrary shapes [12], with any number of additional parameters. The dimension of the parametric space (the number of parameters) dictates the memory cost of the approach; as a circle within a plane is described by three parameters, volumetric data must be maintained. In the context of circle finding, attempts have been made at reducing this dimensionality curse, but at the cost of giving up some capabilities of the traditional Hough transform [13]. Sometimes, parameters can be constrained; for example, a Hough transform with only two parameters is considered in [14] to facilitate gaze tracking, where the circular iris and pupil project to an ellipse that must be detected at video rate.

Since the shape of a snakuscule is circular, it performs best when detecting circular blobs. However, because a snakuscule is region-based, it is also very robust to departures from circularity of the blob it encircles—the actual contour of the blob is immaterial and need not even be determined. Many of the blobs in Fig. 9 are far from being circular, especially the smaller ones, yet Fig. 11 testifies to their successful detection by snakuscules. Meanwhile, the Hough transform usually considers but contours; an additional loss of information must be attributed to the dismissal of grayscale data due to the requirement for binary data. Some robustness could be recovered by coarsening the quantization of the space of parameters, but this coarsening of the quantization would come at the expense of a reduced accuracy. To the contrary, the parameters of the snakuscule remain unquantized since $\mathbf{p}$ and $\mathbf{q}$ are always continuously defined.

C. Circle Fitting

Direct methods to detect circles have been published; they state the problem as finding the circle that best fits a given list of coordinates. An early approach performs an approximate minimization of the mean-square radial error [15]; the analysis of this method was later refined in [16]. These approaches have been extended to the detection of ellipses [17]. The link between coordinate-based and image-based (i.e., Hough-based) approaches has been recently investigated [18].

D. Snakes and Other Deformable Models

Snakes were originally introduced as an energy-minimizing spline guided by external constraint forces and influenced by image forces that pull it toward features such as lines and edges [19]. Several functionals were defined such as the internal energy due to bending, image forces (further categorized as line functional, edge functional, and termination functional), along with external constraint forces. Collectively, they determine the behavior of the snake.

Several parametric descriptions of a snake have been proposed. The most traditional involve points on the contour, sometimes called snaxels [20]. For example, thirty-two points are used in [14] to define a contour-based snake, and least-squares regularization is invoked to collapse the snake into an ellipse. The curve that links snaxels is sometimes a spline [21], but the parameterization may also make use of Fourier descriptors [22]. A relevant issue for some snaxel-based parameterizations is to avoid loops [23], [24]

Ad hoc descriptions that mix different types of curves are also possible. For example, a combination of parabolic sections, punctual objects, and a circle, is introduced in [25] and [26] to model an eye; this description involves eleven parameters.

There, the model is preferentially called a deformable template rather than a snake, although choosing the right terminology is not always straightforward: from the point of view of the measure of fitness, snakes and deformable templates are very similar. They may consider data-dependent terms tied either to image contours [27], [28] or to areas [29], [30], or to both [31], [32]. They may incorporate terms that favor desired traits, such as regularization to promote contour smoothness [33], or dynamic models that adhere to physics-based principles [34].

All these approaches follow a common recipe: choose a model described by a finite number of parameters; decide if and how to penalize some configurations of parameters; choose a measure of fit of the model to the data. Then, given some specific data, tune an initial configuration of parameters to optimize the penalized measure. Such methods go by the name of deformable models [35]. They have been used extensively in the context of medical imaging [36]–[40]. Our snakuscule closely follows this recipe to detect blobs, but is not alone in doing so. In [30] and [36], an edge-based method is proposed to capture ellipses. In [41], an active contour model is encouraged to detect circles thanks to the use of a prior energy term; in addition, repulsive interactions between circles are also considered, reminiscent of Section VII-B. Repulsive forces between snakes is central to the approach discussed in [42].

One difficulty with early edge-based snakes was their dependence on a good initialization. Several solutions have been proposed, such as the introduction of balloon forces to promote expansion of the snake [27], [43], such as sandwiching the contour between a contracting and an expanding snake [44], and, of special interest to snakuscules, such as replacing edge-based measures of fit by measures that take into account at the same time regions inside the contour and outside the contour [45], [46], or such as methods that are based on statistical region models [47] or that are explicitly region-based [29], [32], [48], [49].

E. Applications

In Section VII, we have settled on two common tasks to illustrate the potential usefulness of snakuscules as a general-purpose tool: vessel extraction and cell counting. Meanwhile, numerous studies have focussed on either task and proposed to solve them with specialized methods based on snakes and deformable methods.

The dimensionality of the data dictates two different approaches to vessel extraction. On one hand, when volumetric data are available, the preferred approach is to follow tube cross sections. This was our case in Section VII-A, and can be likened to the medial atoms of [38]. On the other hand, when only a 2-D image is available, a method like that proposed in [40] can be applied. A survey of vessel-extraction techniques can be found in [50] and [51].

Regarding cell detection, a snake-based approach can be found in [52], where, in essence, an active-contour model based on B-spline is applied to the image gradient; the outcome is later simplified to become an ellipse. Regarding cell counting and classification, a method incorporating snakes can be found in [53], where the local maxima of a distance transform applied to a binarized image are used to determine the initial location of the snakes. This results in fewer snake attempts than what we considered in Section VII-B (see Fig. 10). However, the associated binarization process of [53] may result in the loss of some cells; these errors cannot be recovered. By contrast, in our approach we blindly explore the whole image and give equal chances to every cell.

IX. Rattles

We have designed a very simple snake. It depends on no more than two points. They define a pair of concentric disks. The ratio of the disk radii is constant. Ranked by number of parameters, our snake is minuscule. Therefore, we call it a snakuscule. It has two energy terms. Its data term favors a high contrast between the image values averaged over the inner disk and those averaged over the outer annulus. Thus, our snakuscule is a detector of the size and location of circular bright blobs. Its regularization term promotes solutions where its two defining points are horizontal. This effectively removes one degree of freedom. Due to this small number of parameters, the optimizer faces an easy task. We have illustrated the usefulness of the snakuscule for segmenting the aorta and for cell counting. Finally, we invite the adventurous reader to visit the terrarium that we set up in [54], where petting the animals is allowed before downloading them.

In the future, we plan to incorporate a third energy term to express prior knowledge, for example about the expected size of the blobs to detect. The resulting snakuscule will then have acquired the full characteristics of traditional snakes while remaining as simple as possible; this simplicity makes it a good candidate for a didactic introduction to parametric snakes. From a practical point of view, it also yields a most effective algorithm for detecting the location and characterizing the size of bright circular blobs in images.

Appendix

A) Barren Landscape: We can rewrite (1) as a function of the location $\mathbf{y}$ of the snakuscule

$$E_{\text{campester}}(\mathbf{y}) = \int\int_{\|\mathbf{x}\|<R} f(\mathbf{y}+\mathbf{x})dx_1dx_2 - 2\int\int_{\|\mathbf{x}\|<R/\sqrt{2}} f(\mathbf{y}+\mathbf{x})dx_1dx_2.$$

We examine here the conditions under which snakuscules stop crawling. This happens for $\nabla E_{\text{campester}}(\mathbf{y}) = \mathbf{0}$ and yields

$$\int\int_{\|\mathbf{x}\|<R} \nabla f(\mathbf{y}+\mathbf{x})dx_1dx_2 = 2\int\int_{\|\mathbf{x}\|<R/\sqrt{2}} \nabla f(\mathbf{y}+\mathbf{x})dx_1dx_2. \quad (6)$$

As f has not yet been specified, without loss of generality we can set $\mathbf{y} = \mathbf{0}$. With $\mathbf{g}(\rho,\theta) = \nabla f(\mathbf{x})$, we express (6) as

$$\int_{-\pi}^{\pi}\int_{0}^{R} \mathbf{g}(r,\theta)rdrd\theta = 2\int_{-\pi}^{\pi}\int_{0}^{R/\sqrt{2}} \mathbf{g}(r,\theta)rdrd\theta \quad (7)$$

where (ρ, θ) is the polar coordinate that corresponds to the Cartesian coordinate $\mathbf{x}$. We then assume that we can write a component g of $\mathbf{g}$ as a Fourier series in terms of θ. Under appropriate hypotheses, this yields

$$g(r,\theta) = \frac{1}{2} g_0(r) + \sum_{n=1}^{\infty} \left(u_n(r) \cos(n\theta) + v_n(r) \sin(n\theta) \right).$$

Provided the functions u_n and v_n are nonsingular in r, they can be chosen freely because their contribution will vanish under integration over θ. Then, (7) reduces to

$$\int_0^R \mathbf{g}_0(r) r dr = 2 \int_0^{R/\sqrt{2}} \mathbf{g}_0(r) r dr. \tag{8}$$

We now assume that the component $g_0(r)$ can itself be written as the Maclaurin series

$$\forall\, r \in [0, R] : g_0(r) = c_0 + \sum_{n=1}^{\infty} c_n r^n$$

which allows for the explicit integration of (8) and leads to

$$\sum_{n=0}^{\infty} \frac{\mathbf{c}_n}{n+2} R^{n+2} = \sum_{n=0}^{\infty} \frac{\mathbf{c}_n}{n+2} R^{n+2} 2^{-n/2}.$$

As the absence of a preferred location should persist for all R, we deduce that only $\mathbf{c}_0$ can be chosen freely, while $\mathbf{c}_n = \mathbf{0}$ for $n > 0$. As snakuscules go, we finally conclude that the spatial gradient $\boldsymbol{\nabla} f$ of a barren landscape, in which they are unable to orient themselves, necessarily takes the following local form in polar coordinates:

$$\frac{1}{2} \mathbf{c}_0 + \sum_{n=1}^{\infty} \left(\mathbf{u}_n(r) \cos(n\theta) + \mathbf{v}_n(r) \sin(n\theta) \right). \tag{9}$$

B) Cone Zoo: The attentive reader will have observed that the procedure chosen to normalize the energy of the snakuscule, proposed in (2), is not consistent with the linear slope of the cone suggested in Fig. 2. More precisely, if we describe a linear cone in polar coordinates as $f(r,\theta) = r$, then a centered snakuscule exhibits a normalized contrast that remains dependent of its external radius R since $E_{\text{robustus}} = (2\pi/4R^2)\left(\int_{R/\sqrt{2}}^{R} f(r) r dr - \int_0^{R/\sqrt{2}} f(r) r dr \right) = (\pi/12)\left(2 - \sqrt{2}\right) R$. It follows that the desired normalization for a linear cone should rather be proportional to R^3 instead of the proposed R^2.

Meanwhile, the R^2 normalization truly *is* appropriate for other types of cones. The reader can check that

$$f(r,\theta) = C_0 + C_1 \log(r) + \sum_{n \in \mathbb{N} \setminus \{0\}} \left(a_n \cos\left(4n\pi \frac{\log(r)}{\log(2)} \right) + b_n \sin\left(4n\pi \frac{\log(r)}{\log(2)} \right) \right)$$

leads to $E_{\text{campester}} \propto R^2$, where C_0, C_1, a_n, and b_n are arbitrary constants. Moreover, this characterization is complete, in the sense that every cone that leads to $E_{\text{campester}} \propto R^2$ necessarily takes this form. Such cones are highly singular for $r = 0$, not only because of the $\log(r)$ term when $C_1 \neq 0$, but also because of the oscillatory singularities in $\cos(\log(r))$ or $\sin(\log(r))$ when $a_n \neq 0$ or $b_n \neq 0$. However, as snakuscules do not survive shrinking to nothingness anyway (see Section VI), these singularities are irrelevant and the singular section $0 \leq r < \varepsilon$ can appropriately be replaced by a better-behaved section of identical weight, for some arbitrary ε smaller than the smallest viable snakuscule.

So far, we have illustrated the fact that some cones require an R^3 normalization, while others require an R^2 normalization. Thus, the normalization clearly is arbitrary. However, it is necessary, nonetheless, in at least the following situation: Suppose now that the data satisfy $f(r,\theta) = 1 + \text{sign}(r_0 - r)$, which describes an all-or-nothing circular knob of radius r_0. This kind of data is a generic model of common blobs of interest. Without normalization, we can consider four cases—to simplify the discussion, we take for granted that the snakuscule is concentric wit the knob.

1) The snakuscule is too small, with $R < r_0$. Its inner disk does not contrast with its outer annulus because both fully cover the knob, and we observe that $E_{\text{campester}} = 0$.
2) The snakuscule comes short, with $R/\sqrt{2} < r_0 \leq R$. Instead of tightly enclosing the knob, the inner side of the outer annulus partly covers it, so that $E_{\text{campester}} = -2\pi\left(R^2 - r_0^2\right)$.
3) The snakuscule is just the right size. Its outer radius is $R = \sqrt{2} r_0$, so that the minimal energy $E_{\text{campester}} = -2\pi r_0^2$ is attained.
4) The snakuscule is oversized, with $r_0 < R/\sqrt{2}$. The inner disk extends beyond the knob, so that $E_{\text{campester}} = -2\pi r_0^2$ is attained, too.

From this partition of the cases, we deduce that minimizing $E_{\text{campester}}$ does not define a unique snakuscule since the optimal energy is reached even when the snakuscule grows unduly.

To improve on this state of affairs, snakuscules of Brobdingnagian proportions were penalized and encouraged to shrink by considering the generic normalization $E(R,\alpha) = E_{\text{campester}}/R^{\alpha}$, with $0 < \alpha$. In the case of the knob-like data that we're examining in this section, it is easy to verify that $\dot{E}^- = \lim_{R \to \sqrt{2} r_0 - 0} dE(R,\alpha)/dR = \pi(\alpha - 4)\left(\sqrt{2} r_0\right)^{1-\alpha}$ and that $\dot{E}^+ = \lim_{R \to \sqrt{2} r_0 + 0} dE(R,\alpha)/dR = \pi\alpha\left(\sqrt{2} r_0\right)^{1-\alpha}$. To perfectly balance shrinking and expanding requirements, the optimum has to be symmetric, and it is, thus, desirable to impose that $\dot{E}^- = -\dot{E}^+$, which is obtained by setting $\alpha = 2$. This is the evolutionary path that *Serpentulus campester* followed to become *Serpentulus robustus*.

C) Ethology of a Snakuscule: Let f_1 be the first component of the spatial gradient of f. Then, the motive that drives all snakuscule errands is given by (10), shown at the top of the next page.

D) Jousts: Here is the list of rules that govern snakuscules when they enter the fray.

$$
\begin{aligned}
\frac{\partial E_{\text{domesticus}}}{\partial p_1} &= \frac{\partial}{\partial p_1}\frac{1}{\|\mathbf{p}-\mathbf{q}\|^2}\int_{-\pi}^{\pi}\int_{0}^{\|\mathbf{p}-\mathbf{q}\|/2} f\left(\frac{p_1+q_1}{2}+r\cos(\theta),\frac{p_2+q_2}{2}+r\sin(\theta)\right) r\,dr\,d\theta \\
&\quad - \frac{\partial}{\partial p_1}\frac{2}{\|\mathbf{p}-\mathbf{q}\|^2}\int_{-\pi}^{\pi}\int_{0}^{\|\mathbf{p}-\mathbf{q}\|/2\sqrt{2}} f\left(\frac{p_1+q_1}{2}+r\cos(\theta),\frac{p_2+q_2}{2}+r\sin(\theta)\right) r\,dr\,d\theta \\
&\quad + \lambda\frac{\partial}{\partial p_1}\frac{(p_2-q_2)^2}{\|\mathbf{p}-\mathbf{q}\|^2} \\
&= \frac{-2(p_1-q_1)}{\|\mathbf{p}-\mathbf{q}\|^2}E_{\text{robustus}} \\
&\quad - \lambda\frac{(p_1-q_1)(p_2-q_2)^2}{\|\mathbf{p}-\mathbf{q}\|^4} + \frac{1}{\|\mathbf{p}-\mathbf{q}\|^2}\int_{-\pi}^{\pi}\int_{0}^{\|\mathbf{p}-\mathbf{q}\|/2} f_1\left(\frac{p_1+q_1}{2}+r\cos(\theta),\frac{p_2+q_2}{2}+r\sin(\theta)\right)\frac{1}{2}r\,dr\,d\theta \\
&\quad - \frac{2}{\|\mathbf{p}-\mathbf{q}\|^2}\int_{-\pi}^{\pi}\int_{0}^{\|\mathbf{p}-\mathbf{q}\|/2\sqrt{2}} f_1\left(\frac{p_1+q_1}{2}+r\cos(\theta),\frac{p_2+q_2}{2}+r\sin(\theta)\right)\frac{1}{2}r\,dr\,d\theta \\
&\quad + \frac{1}{\|\mathbf{p}-\mathbf{q}\|^2}\int_{-\pi}^{\pi} f\left(\frac{p_1+q_1}{2}+\frac{\|\mathbf{p}-\mathbf{q}\|}{2}\cos(\theta),\frac{p_2+q_2}{2}+\frac{\|\mathbf{p}-\mathbf{q}\|}{2}\sin(\theta)\right)\frac{p_1-q_1}{4}d\theta \\
&\quad - \frac{2}{\|\mathbf{p}-\mathbf{q}\|^2}\int_{-\pi}^{\pi} f\left(\frac{p_1+q_1}{2}+\frac{\|\mathbf{p}-\mathbf{q}\|}{2\sqrt{2}}\cos(\theta),\frac{p_2+q_2}{2}+\frac{\|\mathbf{p}-\mathbf{q}\|}{2\sqrt{2}}\sin(\theta)\right)\frac{p_1-q_1}{8}d\theta. \qquad (10)
\end{aligned}
$$

1) Pick an arbitrary number of iterations N, and an arbitrary increase ΔN. Choose an energy threshold E_0. Arrange the swarm members in their initial configuration.
2) Update the current configuration of the remaining snakuscules by individually optimizing them for the current number of iterations N (but stop optimizing a snakuscule in case it converges early).
3) Establish a sequential list of all possible pairs of remaining snakuscules, irrespective of whether they have already converged or not.
4) Scan the list, but skip every pair for which at least one of its members has already been removed.
5) Check whether the central disks of the current pair of snakuscules overlap, which happens for $\|x_0'' - x_0'\| < \max(R'', R')/\sqrt{2}$.
6) Whenever an overlap occurs, compare the energy of the two snakuscules in the pair and remove that snakuscule that has the worst (largest) energy.
7) Increase the number of iterations $N \leftarrow N + \Delta N$.
8) Repeat Steps 2)–7) until all remaining snakuscules have converged.
9) Finally, remove all those snakuscules for which $E_0 < E_{\text{vulgaris}}$.

ACKNOWLEDGMENT

This work was supported by the Center for Biomedical Imaging (CIBM) of the Geneva-Lausanne Universities and the EPFL, as well as by the Hasler, Leenaards, and Louis-Jeantet Foundations.

REFERENCES

[1] M. V. Martialis, "Epigrammata liber I," *38–104 AD, Epigramma IX*.
[2] J. S. Socha, T. O'Dempsey, and M. LaBarbera, "A 3-D kinematic analysis of gliding in a flying snake, *Chrysopelea paradisi*," *J. Exp. Biol.*, vol. 208, no. 10, pp. 1817–1833, May 2005.
[3] G. Perec, "Experimental demonstration of the tomatotopic organization in the soprano (*Cantatrix Sopranica L.*)," *Banana Split*, vol. 2, pp. 63–74, 1980, Aix-en-Provence, France.
[4] J. de la Fontaine, "La Grenouille qui se veut faire aussi grosse que le Bœuf," *1668, Livre I, Fable 3*.
[5] S. W. Hawking, "Black hole explosions?," *Nature*, vol. 248, no. 5443, pp. 30–31, Mar. 1974.
[6] B. Zavidovique, X. Merlo, and L. Foulloy, "Hey robot,…looking for cones?," in *Proc. IEEE Computer Society Conf. Computer Vision and Pattern Recognition*, San Francisco, CA, Jun. 19–23, 1985, pp. 379–381.
[7] M. A. Branham and M. D. Greenfield, "Flashing males win mate success," *Nature*, vol. 381, no. 6585, pp. 745–746, Jun. 1996

MORE REFERENCES.

[8] D. S. Bright and E. B. Steel, "Two-dimensional top hat filter for extracting spots and spheres from digital images," *J. Microsc.*, vol. 146, no. 2, pp. 191–200, May 1987.
[9] P. V. C. Hough, "Method and means for recognizing complex patterns," U. S. Patent 3 069 654, 1962.
[10] R. O. Duda and P. E. Hart, "Use of the Hough transformation to detect lines and curves in pictures," *Commun. ACM*, vol. 15, no. 1, pp. 11–15, Jan. 1972.
[11] C. Kimme, D. Ballard, and J. Sklansky, "Finding circles by an array of accumulators," *Commun. ACM*, vol. 18, no. 2, pp. 120–122, Feb. 1975.
[12] D. H. Ballard, "Generalizing the Hough transform to detect arbitrary shapes," *Pattern Recognit.*, vol. 13, no. 2, pp. 111–122, 1981.
[13] R. S. Conker, "A dual plane variation of the Hough transform for detecting non-concentric circles of different radii," *Comput. Vis., Graph., Image Process.*, vol. 43, no. 2, pp. 115–132, Aug. 1988.
[14] D. Young, H. Tunley, and R. Samuels, "Specialised Hough transform and active contour methods for real-time eye tracking," Cogn. Sci. Res. Papers 386, Univ. Sussex. U.K., 1995.
[15] I. Kåsa, "A circle fitting procedure and its error analysis," *IEEE Trans. Instrum. Meas.*, vol. 25, no. 3, pp. 8–14, Mar. 1976.
[16] C. A. Corral and C. S. Lindquist, "On implementing Kåsa's circle fit procedure," *IEEE Trans. Instrum. Meas.*, vol. 47, no. 6, pp. 789–795, Jun. 1998.
[17] A. Fitzgibbon, M. Pilu, and R. B. Fisher, "Direct least square fitting of ellipses," *IEEE Trans. Instrum. Meas.*, vol. 21, no. 5, pp. 476–480, May 1999.

[18] E. E. Zelniker and I. V. L. Clarkson, "Maximum-likelihood estimation of circle parameters via convolution," *IEEE Trans. Image Process.*, vol. 15, pp. 865–876, Apr. 2006.
[19] M. Kass, A. Witkin, and D. Terzopoulos, "Snakes: Active contour models," in *Proc. 1st Int. Conf. Computer Vision*, London, U.K., Jun. 8–11, 1987, pp. 259–268.
[20] K. Sobottka and I. Pitas, "Segmentation and tracking of faces in color images," in *Proc. 2nd Int. Conf. Automatic Face and Gesture Recognition*, Killington, VT, Oct. 14–16, 1996, pp. 236–241.
[21] S. Menet, P. Saint-Marc, and G. Medioni, "B-snakes: Implementation and application to stereo," in *Proc. DARPA Image Understanding Workshop*, Pittsburgh, PA, Sep. 11–13, 1990, pp. 720–726.
[22] G. L. Scott, "The alternative snake—And other animals," in *Proc. 3rd Alvey Vision Conf.*, Cambridge, U.K., Sep. 15–17, 1987, pp. 341–347.
[23] L. Ji and H. Yan, "Loop-free snakes for image segmentation," in *Proc. IEEE Int. Conf. Image Processing*, Kobe, Japan, Oct. 24–28, 1999, vol. 3, pp. 193–197.
[24] M. Jacob, T. Blu, and M. Unser, "Efficient energies and algorithms for parametric snakes," *IEEE Trans. Image Process.*, vol. 13, no. 9, pp. 1231–1244, Sep. 2004.
[25] A. L. Yuille, D. S. Cohen, and P. W. Hallinan, "Feature extraction from faces using deformable templates," in *Proc. IEEE Computer Society Conf. Computer Vision and Pattern Recognition*, San Diego, CA, Jun. 4–8, 1989, pp. 104–109.
[26] A. L. Yuille, P. W. Hallinan, and D. S. Cohen, "Feature extraction from faces using deformable templates," *Int. J. Comput. Vis.*, vol. 8, no. 2, pp. 99–111, Aug. 1992.
[27] L. D. Cohen, "On active contour models and balloons," *CVGIP: Image Understand.*, vol. 53, no. 2, pp. 211–218, Mar. 1991.
[28] M. Worring, A. W. M. Smeulders, L. H. Staib, and J. S. Duncan, "Parameterized feasible boundaries in gradient vector fields," *Comput. Vis. Image Understand.*, vol. 63, no. 1, pp. 135–144, Jan. 1996.
[29] R. Ronfard, "Region-based strategies for active contour models," *Int. J. Comput. Vis.*, vol. 13, no. 2, pp. 229–251, Oct. 1994.
[30] P. Lipson, A. L. Yuille, D. O'Keeffe, J. Cavanough, J. Taaffe, and D. Rosenthal, "Deformable templates for features extraction from medical images," *Lecture Notes Comput. Sci.*, vol. 427, pp. 413–417, 1990.
[31] A. Chakraborty, L. H. Staib, and J. S. Duncan, "An integrated approach to boundary finding in medical images," in *Proc. IEEE Workshop on Biomedical Image Analysis*, Seattle, WA, Jun. 24–25, 1994, pp. 13–22.
[32] A. Chakraborty, L. H. Staib, and J. S. Duncan, "Deformable boundary finding in medical images by integrating gradient and region information," *IEEE Trans. Med. Imag.*, vol. 15, no. 6, pp. 859–870, Dec. 1996.
[33] D. Mumford and J. Shah, "Boundary detection by minimizing functionals, I," in *Proc. IEEE Computer Society Conf. Computer Vision and Pattern Recognition*, San Francisco, CA, Jun. 19–23, 1985, pp. 22–26.
[34] D. Metaxas and D. Terzopoulos, "Shape and nonrigid motion estimation through physics-based synthesis," *IEEE Trans. Pattern Anal. Mach. Intell.*, vol. 15, no. 6, pp. 580–591, Jun. 1993.
[35] T. McInerney and D. Terzopoulos, "Deformable models in medical image analysis: A survey," *Med. Image Anal.*, vol. 1, no. 2, pp. 91–108, Jun. 1996.
[36] P. Lipson, A. L. Yuille, D. O'Keeffe, J. Cavanough, J. Taaffe, and D. Rosenthal, "Automated bone density calculation using feature extraction by deformable templates," in *Proc. 1st conf. Visualization in Biomedical Computing*, Atlanta, GA, May 22–25, 1990, pp. 477–484.
[37] X. Wang and W. G. Wee, "A new deformable contour method," in *Proc. 10th Int. Conf. Image Analysis and Processing*, Venice, Italy, Sep. 27–29, 1999, pp. 430–435.
[38] Y. Fridman, S. M. Pizer, S. Aylward, and E. Bullitt, "Segmenting 3D branching tubular structures using cores," *Lecture Notes Comput. Sci.*, vol. 2879, pp. 570–577, 2003.
[39] X. Wang, L. He, Y. Tang, and W. G. Wee, "A divide and conquer deformable contour method with a model based searching algorithm," *IEEE Trans. Syst., Man, Cybern. B, Cybern.*, vol. 33, no. 5, pp. 738–751, Oct. 2003.
[40] G. Yu, P. Lin, P. Li, and Z. Bian, "Region-based vessel segmentation using level set framework," *Int. J. Control, Autom., Syst.*, vol. 4, no. 5, pp. 660–667, Oct. 2006.
[41] P. Horváth, I. Jermyn, Z. Kato, and J. Zerubia, "A higher-order active contour model for tree detection," in *Proc. 18th Int. Conf. Pattern Recognition*, Hong Kong, Aug. 20–24, 2006, pp. 130–133.
[42] R. Yang, M. Mirmehdi, and X. Xie, "A charged active contour based on electrostatics," *Lecture Notes Comput. Sci.*, vol. 4179, pp. 173–184, 2006.
[43] S. C. Zhu and A. L. Yuille, "Region competition: Unifying snakes, region growing, and Bayes/MDL for multiband image segmentation," *IEEE Trans. Pattern Anal. Mach. Intell.*, vol. 18, no. 9, pp. 884–900, Sep. 1996.
[44] S. R. Gunn and M. S. Nixon, "A robust snake implementation; A dual active contour," *IEEE Trans. Pattern Anal. Mach. Intell.*, vol. 19, no. 1, pp. 63–68, Jan. 1997.
[45] T. Chan and L. Vese, "An active contour model without edges," *Lecture Notes Comput. Sci.*, vol. 1682, pp. 141–151, 1999.
[46] T. F. Chan and L. A. Vese, "Active contours without edges," *IEEE Trans. Image Process.*, vol. 10, no. 2, pp. 266–277, Feb. 2001.
[47] M. T. de Figueiredo and J. M. N. Leitão, "Bayesian estimation of ventricular contours in angiographic images," *IEEE Trans. Med. Imag.*, vol. 11, no. 9, pp. 416–429, Sep. 1992.
[48] M. Jacob, T. Blu, and M. Unser, M. Sonka and K. M. Hanson, Eds., "A unifying approach and interface for spline-based snakes," in *Proc. Progress in Biomedical Optics and Imaging*, San Diego, CA, Feb. 19–22, 2001, vol. 4322, pp. 340–347.
[49] X. Xie and M. Mirmehdi, "RAGS: Region-aided geometric snake," *IEEE Trans. Image Process.*, vol. 13, no. 5, pp. 640–652, May 2004.
[50] C. Kirbas and F. K. H. Quek, "Vessel extraction techniques and algorithms: A survey," in *Proc. 3rd IEEE Symp. BioInformatics and BioEngineering*, Bethesda, MD, Mar. 10–12, 2003, pp. 238–245.
[51] C. Kirbas and F. Quek, "A review of vessel extraction techniques and algorithms," *ACM Comput. Surv.*, vol. 36, no. 2, pp. 81–121, Jun. 2004.
[52] G. Dong, N. Ray, and S. T. Acton, "Intravital leukocyte detection using the gradient inverse coefficient of variation," *IEEE Trans. Med. Imag.*, vol. 24, no. 7, pp. 910–924, Jul. 2005.
[53] G. Ongun, U. Halici, K. Leblebicioglu, V. Atalay, M. Beksac, and S. Beksac, "An automated differential blood count system," in *Proc. 23rd Annu. EMBS Int. Conf.*, Istanbul, Turkey, Oct. 25–28, 2001, pp. 2583–2586.
[54] P. Thévenaz, Snakuscule Software Availability 2006 [Online]. Available: http://bigwww.epfl.ch/thevenaz/snakuscule/

Philippe Thévenaz was born in 1962 in Lausanne, Switzerland. He graduated from the École polytechnique fédérale de Lausanne (EPFL), Switzerland, with a diploma in microengineering in January 1986 and received the Ph.D. degree, with a thesis on the use of the linear prediction residue for text-independent speaker recognition, in June 1993.

He joined the Institute of Microtechnology (IMT), University of Neuchâtel, Switzerland, where he worked in the domain of image processing (optical flow) and in the domain of speech processing (speech coding and speaker recognition). He was a Visiting Fellow with the Biomedical Engineering and Instrumentation Program, National Institutes of Health (NIH), Bethesda, MD, where he developed research interests that include splines and multiresolution signal representations, geometric image transformations, and biomedical image registration. Since 1998, he has been with the EPFL as a Senior Researcher.

Michael Unser (M'89–SM'94–F'99) received the M.S. *(summa cum laude)* and Ph.D. degrees in electrical engineering from the Swiss Federal Institute of Technology (EPFL), Lausanne, Switzerland, in 1981 and 1984, respectively.

From 1985 to 1997, he was a Scientist with the National Institutes of Health, Bethesda, MD. He is now a Professor and Director of the Biomedical Imaging Group, EPFL. His main research topics are biomedical image processing, splines, and wavelets. He is the author of over 150 published journal papers in these areas.

Dr. Unser has been actively involved with the IEEE TRANSACTIONS ON MEDICAL IMAGING, holding the positions of Associate Editor (1999–2002 and 2006–present), member of steering committee, and Associate Editor-in-Chief (2003–2005). He has acted as an Associate Editor or member of the editorial board for eight more international journals, including the *IEEE Signal Processing Magazine*, the IEEE TRANSACTIONS ON IMAGE PROCESSING (1992–1995), and the IEEE SIGNAL PROCESSING LETTERS (1994–1998). He organized the first IEEE International Symposium on Biomedical Imaging (ISBI 2002). He was the founding Chair of the technical committee of the IEEE-SP Society on Bio Imaging and Signal Processing (BISP), and he currently chairs the ISBI steering committee. He is a recipient of three Best Paper Awards from the IEEE Signal Processing Society.